Journal of the Mechanics and Physics of Solids 57 (2009) 744–761

Contents lists available at ScienceDirect

Journal of the Mechanics and Physics of Solids

journal homepage: www.elsevier.com/locate/jmps

Diffusionally assisted grain-boundary sliding and viscoelasticity of polycrystals

S.J.S. Morris [a,*], Ian Jackson [b]

[a] Department of Mechanical Engineering, University of California, Berkeley 94720, USA
[b] Research School of Earth Sciences, Australian National University, Canberra, ACT 0200, Australia

ARTICLE INFO

Article history:
Received 22 February 2008
Received in revised form
3 December 2008
Accepted 19 December 2008

Keywords:
Grain boundaries
Diffusion, Surface
Stress concentrations
Creep
Q (quality factor)

ABSTRACT

Motivated by recent attenuation experiments on finely grained samples, we reanalyse the Raj–Ashby model of grain-boundary sliding. Two linearly elastic layers having finite thickness and identical elastic constants are separated by an interface (grain boundary) whose location is a given periodic function of position. Dissipation is confined to that interfacial region. It is caused by two mechanisms: a slip (boundary sliding) viscosity, and grain-boundary diffusion, with corresponding Maxwell relaxation times t_v and t_d. Owing to the assumption of a given, time-independent interface, the resulting boundary-value problem (b.v.p.) is linear and time-separable. The response to time-periodic forcing depends on angular frequency ω, on the ratio $\mathscr{M} = t_v/t_d$ of Maxwell times, and on the characteristic interface slope. The b.v.p. is solved using a perturbation method valid for small slopes. To relate features of the mechanical loss spectrum previously studied in isolation, we first discuss the solution as a function of $\mathscr{M}$. Motivated by experiments, we then emphasize the case $\mathscr{M} \ll 1$ in which the relaxation times are widely separated. The loss spectrum then always has two major features: a frequency band $1 \ll \omega t_d \ll \mathscr{M}^{-1}$ within which the loss varies relatively weakly with ω; and a loss maximum at $\omega t_d \sim \mathscr{M}^{-1}$ due to the slip viscosity. If corners on the interface are sufficiently rounded, those two universal features are separated by a third feature: between them, there is a strong minimum whose location is (entirely) independent of slip viscosity. The existence of that minimum has not previously been reported. These features are likely to occur even in solutions for finite interface slopes, because they are a consequence of the separation of timescales. The precise form of the spectrum in the weakly varying band must, however, be slope-dependent because it is controlled by stress singularities occurring at corners, and the strength of those singularities depends on the angle subtended by the corner.

1. Introduction

The high-temperature breakdown of perfectly elastic behaviour in finely grained solids is usually attributed to grain-boundary sliding facilitated by the low effective viscosity of the thin grain-boundary region. Recent experimental studies of high-temperature viscoelastic relaxation in finely grained samples of both ceramic and geological materials suggest the following relation between the observed relaxation and the grain-boundary microstructure (Jackson et al., 2006;

* Corresponding author.
E-mail address: morris@me.berkeley.edu (S.J.S. Morris).

0022-5096/$ - see front matter © 2008 Elsevier Ltd. All rights reserved.
doi:10.1016/j.jmps.2008.12.006

Barnhoorn et al., 2007). For genuinely single-phase polycrystals, the dissipation varies monotonically across a wide range of frequency and temperature, behaviour commonly described as 'high-temperature background' (Nowick and Berry, 1972). By contrast, the presence of a dispersed secondary phase of low viscosity is typically associated with additional structure, such as a local maximum or a kink in the spectrum.

Sliding on a non-plane grain boundary produces incompatibilities that must be accommodated under conditions of low stress either by elastic distortion of the sliding grains or by diffusional transport of matter along the boundary. Grain-boundary sliding with elastic accommodation, and the diffusionally accommodated sliding responsible for transient and steady-state diffusional creep have been separately addressed by Raj and Ashby (1971), Raj (1975) and Mosher and Raj (1974). These models have been widely invoked in the interpretation of experimental data (e.g. Pezzotti et al., 1996; Gribb and Cooper, 1998; Cooper (2002); Lakki et al., 1999; Jackson et al., 2002; Faul et al., 2004). However, important features of the experimental data, notably (a) the mild frequency dependence of the dissipation background, and (b) the absence of a peak attributable to elastically accommodated grain-boundary sliding in the single-phase materials, are at odds with the classical models.

Those difficulties have motivated us to reformulate, and reanalyse the Raj–Ashby model. For the first time, we pose a complete boundary value problem (b.v.p.) for the model. Because we give the first solution including the simultaneous action of diffusion and a slip viscosity attributed to the grain interface, we are able to show the relation between phenomena previously studied in isolation. Our solution is explicit, and we give simplified forms for limiting cases. Though our solution is limited to interface topography having small characteristic slope, it is rigorous and provides a standard for testing the numerical solutions needed for more complex geometries.

In Section 2 we state the b.v.p. The model sample consists of two linearly elastic layers of finite thickness having identical elastic rigidityμ and Poisson ratio ν. Those layers, modelling the crystal grains, are separated by an interface whose location is a prescribed function of position. Dissipation is confined to the interfacial region. There it occurs by two processes: viscous slip as discussed by Mosher and Raj (1974), and grain-boundary diffusion. As there are two dissipative processes, the model contains two timescales: they are Maxwell relaxation times based on μ, the slip (boundary) viscosity η' and the viscosity η for the steady-state Coble creep that is one of the solutions of the model (Raj, 1975; Kim et al., 2005).

In Section 3, we expand the solution as a power series in the characteristic interface slope ε. Our method differs from that of Raj–Ashby because we have a well-defined base state for the case $\varepsilon = 0$ describing a plane interface. In that state, the elastic layers are in simple shear; they slip along the interface at a rate set by η'. The interaction of grain elasticity with slip viscosity causes the sample as a whole to behave as a Maxwell solid at this order of approximation. We proceed to $O(\varepsilon^2)$ in the perturbation expansion, and obtain an explicit expression giving the complex sample rigidity G as a function of frequency. In Section 4, we collect our analytical results, and in the rest of the paper, we discuss their implications.

In Section 5 we show that unless the two timescales in the model differ by orders of magnitude, the model cannot explain the mild frequency dependence of the dissipation background. We also show that by allowing the simultaneous action of diffusion and slip viscosity, we ensure that the power series solution satisfies a basic criterion: because allowing slip on interfaces cannot strengthen the solid, the magnitude $|G|$ of the complex sample rigidity cannot exceed the rigidity of the individual grains. That criterion is not satisfied by previous versions of the Raj–Ashby model in which the base state is implicitly assumed to be a piecewise rigid motion.

In Section 6, we set the slip viscosity $\eta' = 0$, and treat the case of diffusionally assisted inviscid grain-boundary sliding. The model now has a single timescale, namely the Maxwell relaxation time η/μ based on the viscosity for steady-state Coble creep. We derive simple formulae giving the low-frequency and high-frequency asymptotes to our numerical solution for G. The high-frequency limit is of particular interest in experimental studies of attenuation in mantle materials such as olivine; at seismic frequencies, the dimensionless angular forcing frequency $\omega\eta/\mu$ ranges from $\sim$1 to 10^8 (Morris and Jackson, 2008). In Section 6 we also determine the creep function for our solution.

Because our results for the short-time behaviour of the creep function, and the corresponding high-frequency behaviour of G differ from results published, respectively, by Raj (1975), and by Gribb and Cooper (1998), we note that the asymptotes derived analytically by us agree well with our numerical solutions of the model. Moreover, in Section 7, we use scaling to explain the physical basis of the new high-frequency asymptote, so that all aspects of our new analysis are consistent both mathematically and physically. The scaling arguments are used to clarify the importance of contact singularities in controlling the high-frequency behaviour of the loss spectrum of finely grained materials. In Section 8, we summarize our chief results. Throughout this work, asterisks are used to denote dimensional variables.

2. Boundary-value problem

2.1. Formulation

Fig. 1 shows the geometry of the model. The sample consists of two perfectly elastic grains separated by an interface S_I. In the figure, heavy solid curves show the sample boundary, and that interface. Because in attenuation experiments the total strain, including the creep strain, is small, we follow Raj and Ashby (1971) in assuming the (dimensional) interface location $f_*(x_*)$ to be a given periodic function of x_*; f_* has zero spatial mean and, as shown in the figure, wavelength $2\pi/\xi$. Unit tangent and unit normal vectors for the interface are, respectively, denoted by $\boldsymbol{e_s}$ and $\boldsymbol{e_n}$. Unit vectors in the coordinate

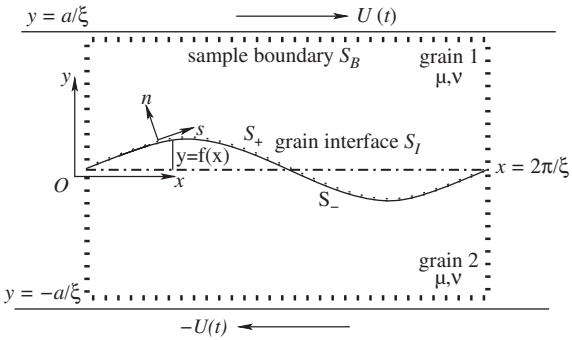

Fig. 1. Definition sketch. . . ., surfaces bounding one wavelength of a grain. – · –, spatial mean location of the grain interface.

directions are denoted by $\boldsymbol{e_x}$, $\boldsymbol{e_y}$, $\boldsymbol{e_z}$. The total sample thickness is $2a/\xi$, so the dimensionless quantity $2a$ is the product of sample thickness with the fundamental wavenumber of the topography. At the sample boundaries S_B at $y_* = \pm a/\xi$, a displacement $\pm U_*(t)\boldsymbol{e_x}$ is imposed. We assume plane deformation, so the (dimensional) stress tensor and displacement vector, respectively, have components σ^*_{ij}, and $u^*_1 = u^*$, $u^*_2 = v^*$, $u_3 = 0$. The deformation (strain) tensor is denoted by e^*_{ij}. Lastly, in the figure, light broken curves show control surfaces S_+ and S_- lying, respectively, just above, and just below, S_I; those control surfaces are used in the discussion of energetics given as Appendix B.

We take the grains to be Hookean solids with common elastic rigidity μ and Poisson ratio ν. Constitutive laws are also needed to relate the discontinuities in the tangential and normal components u^*_s, u^*_n of displacement to the corresponding stress components σ^*_{ns}, σ^*_{nn}; as usual in continuum mechanics, tensile stresses are taken as positive. With $\dot{\boldsymbol{u}}^* = \partial \boldsymbol{u}^*/\partial t^*$, the first constitutive law is

$$\ell\sigma^*_{ns} = \eta'[\dot{u}^*_s]. \tag{1}$$

According to this equation, at the interface, the shear stress is proportional to the discontinuity in tangential velocity. An interfacial area element thus behaves as if the grains were separated by a thin film of Newtonian liquid of (constant) characteristic thickness ℓ, and viscosity η' (Lifshitz, 1963; Raj and Ashby, 1971).

The second constitutive equation is obtained in two steps. First, the volume flow rate j_* (per unit z-length) along the interface by grain-boundary diffusion is related to the tangential derivative of σ^*_{nn} by a form of Fick's law, namely

$$j_* = \frac{V\ell D}{kT}\frac{\mathrm{d}\sigma^*_{nn}}{\mathrm{d}s_*}$$

(Lifshitz, 1963; Raj and Ashby, 1971); V, D and k denote, respectively, the molecular volume, grain-boundary diffusivity and Boltzmann constant. By definition, j_* has dimensions of L^2/T. (For simplicity, we do not include volume diffusion here. Raj and Ashby (1971) show its effect to be negligible if the wavelength and volume diffusivity D_v satisfy $2\pi/\xi \ll \ell D/D_v$. That condition is satisfied in typical attenuation experiments on finely grained samples (e.g. Jackson et al., 2002). Moreover, the physical ideas identified in the abstract would be obscured by the complications needed to include volume diffusion.)

Combining Fick's law with the interfacial mass balance, namely $[\dot{u}^*_n] + \mathrm{d}j_*/\mathrm{d}s_* = 0$, we obtain the evolution equation for the discontinuity in u_n, namely:

$$[\dot{u}^*_n] + \frac{V\ell D}{kT}\frac{\mathrm{d}^2\sigma^*_{nn}}{\mathrm{d}s^2_*} = 0. \tag{2}$$

From parameters contained in Eqs. (1) and (2), the following times can be formed:

$$t_\mathrm{v} = \eta'/\xi\ell\mu, \quad t_d = kT/\mu V\ell D\xi^3 \tag{3a,b}$$

(Mosher and Raj, 1974; Raj, 1975). The viscous scale t_v is the timescale on which the two sides of Eq. (1) balance, i.e. t_v is the Maxwell relaxation time based on η' and μ. The diffusion scale t_d is the timescale on which the terms in Eq. (2) balance if derivatives along the interface scale with wavelength. As a result, for dimensional angular frequency $\omega_* \gg t_d^{-1}$, diffusion can only be significant at scales small compared with the wavelength. On an interface with corners, the effect of diffusion is then limited to within a distance $\sim\ell_d$ of the corner, where

$$\ell_d = (\mu V\ell D/kT\omega_*)^{1/3}. \tag{4}$$

At the end of this section, we show that t_d can also be interpreted as a Maxwell relaxation scale based on μ and η, i.e. the viscosity for steady-state Coble creep with zero shear stress on the interface.

We define dimensionless variables (without asterisks):

$$(x_*, y_*) = (x, y)/\xi, \quad \boldsymbol{u}_* = U_s \boldsymbol{u}, \quad f_* = \varepsilon f/\xi,$$
$$\sigma_{ij*} = \mu \xi U_s \sigma_{ij}, \quad t_* = t_d\, t, \quad j_* = j U_s/t_d \xi. \tag{5}$$

U_s is the characteristic displacement imposed at the sample boundaries. As previously defined, ξ is the fundamental wavenumber of the interface topography, so that ε is the characteristic interface slope; specifically, $\mathrm{d}f_*/\mathrm{d}x_* = \varepsilon f'(x)$. Throughout this work f' denotes the dimensionless derivative $\mathrm{d}f/\mathrm{d}x$.

The dimensionless b.v.p. is as follows:

$$\text{within each grain} \quad \theta = \nabla \cdot \boldsymbol{u}, \tag{6a}$$
$$\nabla\theta + (1-2\nu)\nabla^2 \boldsymbol{u} = 0; \tag{6b}$$
$$\text{on } |y| = a, \quad u = \pm U(t), \quad v = 0; \tag{6c,d}$$
$$\text{on } y = \varepsilon f(x), \quad [\sigma_{nn}] = 0 = [\sigma_{ns}], \tag{6e,f}$$
$$[\dot{u}_n] + \frac{\mathrm{d}^2 \sigma_{nn}}{\mathrm{d}s^2} = 0, \tag{6g}$$
$$\mathscr{M}[\dot{u}_s] = \sigma_{ns}. \tag{6h}$$

In (6h), the parameter $\mathscr{M} = t_v/t_d$ is the ratio of the Maxwell times, i.e.

$$\mathscr{M} = \eta' V D \xi^2/kT. \tag{6i}$$

The limit $\mathscr{M} \to 0$ (fixed frequency) corresponds to an effectively inviscid interface, i.e. to one on which $\sigma_{ns} = 0$.

The object of the calculation is to find the x-averaged stress τ that must be applied at the boundary to drive the boundary displacement $U(t)$; specifically, we determine

$$\tau(t) = \frac{1}{2\pi}\int_0^{2\pi} \sigma_{xy}(x, a, t)\, \mathrm{d}x. \tag{7}$$

Two aspects of the b.v.p. (6) are important in interpreting the solution later. First, within the elastic layers, the deformation is governed by the Navier–Cauchy equations (6a) and (6b) describing elastostatic equilibrium. That assumption is appropriate because in the systems of interest, the grain size is small compared with the wavelength of a shear wave. As a result of this simplification, time-derivatives enter the b.v.p. only through the interfacial conditions (6g) and (6h). We call those equations, respectively, the diffusion, and the slip, boundary conditions.

Secondly, the b.v.p. is linear, because the location $y = \varepsilon f(x)$ of the grain interface is prescribed, and independent of time. Owing to the time-invariance of the interface, b.v.p. (6) is separable with respect to time. In particular, an imposed boundary displacement of the form

$$U = \hat{U}(\omega)\mathrm{e}^{\mathrm{i}\omega t} \tag{8a}$$

causes an x-averaged shear stress τ of the form

$$\tau = \hat{\tau}(\omega)\mathrm{e}^{\mathrm{i}\omega t}. \tag{8b}$$

With $\hat{\gamma} = \hat{U}/a$ being the Fourier transform of the dimensionless sample strain, the complex rigidity G is defined by

$$G = \hat{\tau}(\omega)/\hat{\gamma}(\omega). \tag{8c}$$

The mechanical loss $\mathscr{L}$ is defined by the equation

$$\mathscr{L} = \tan \arg G \tag{9}$$

(Findley et al., 1989, p. 93). We note that if the material can be modelled as a network of linear springs and dampers, $\mathscr{L}$ equals the ratio of the mechanical energy dissipated per cycle to 4π times the mean strain energy stored within the sample (Bland, 1960, p. 43; O'Connell and Budiansky, 1978).

Time-invariance of the interface has another important consequence. It strongly constrains the smoothing effect of diffusion. For example, let us suppose that an initially undeformed sample is subject to a Heaviside unit step in applied stress. For $t \ll t_d$, diffusion is inoperative, and boundary condition (6g) simplifies to $[\dot{u}_n] = 0$. At grain corners, $\boldsymbol{e_n}$ is discontinuous, and so too is the displacement field $\boldsymbol{u}$. As a result, the stress there is singular for $t \ll t_d$. Subsequently, i.e. for $t \sim t_d$, the two terms in (6g) can balance; diffusion acts on the timescale t_d to relieve the stress concentrations. But owing to the time-invariant interface, diffusion relaxes that singularity not by reshaping the interface, but rather by modifying the displacement field. Because this model is not described by Fick's second law of diffusion, there is no a priori reason to expect that an initial stress singularity will decay according to the $t^{-1/2}$ relation claimed by Gribb and Cooper (1998). In fact, even in steady-state creep, where diffusion acts over the whole grain boundary, a weak singularity (discontinuity) in normal stress persists at corners, as we now discuss.

2.2. Steady-state solution

If the applied stress is a Heaviside unit step in t, b.v.p. (6) admits the solution

$$\boldsymbol{u} = \pm \dot{U}_\infty t \boldsymbol{e_x} + \boldsymbol{u}'(x,y), \tag{10}$$

where the constant $\dot{U}_\infty$ is the steady (Coble) creep rate, and the second term is independent of t. (Because the transient response decays on the diffusion timescale t_d, Eq. (10) describes the displacement for $t_* \gg t_d$.) The first term in (10) describes a piecewise rigid translation, and the stress needed to induce that displacement is obtained from (6). It is not, however, necessary to determine the stress distribution within the grains in order to find the boundary stress τ. For, as noted by Raj–Ashby (p. 1117), in this case the interfacial conditions (6g) and (6h) completely determine the stress distribution on the grain interface, and the desired stress τ is then determined from the condition that the grains are in mechanical equilibrium. The steady displacement field $\boldsymbol{u}'$ responds passively to the stress imposed at the grain interface. That insight is used e.g. by Hazzledine and Schneibel (1993) and Ford et al. (2004) to study steady-state creep in polycrystalline arrays; in their configuration, the rigid-body motion described by the first term in (10) also includes a rigid-body rotation.

We may note that this solution describing steady-state creep has a weak stress singularity at corners. Specifically, for a sawtooth interface, σ_{nn} can be shown to vary parabolically with x (Raj, 1975, p. 1501; Kim et al., 2005, eq. 9). As a result, $\mathrm{d}^2\sigma_{nn}/\mathrm{d}s^2$ is discontinuous at corners, so that time-invariance of the grain interface has the consequence that diffusion weakens the singularity in $\boldsymbol{u}$ without removing it. As that is so for the case of steady-state creep in which the entire grain boundary is affected by diffusion, we expect (and find) both transient creep and attenuation to be even more strongly affected by stress concentrations at corners.

Eq. (10) also allows t_d to be interpreted as the Maxwell relaxation time η/μ for the case $\mathscr{M} = 0$, i.e. for zero shear stress on the interface. From b.v.p. (6), we see that the creep rate $\dot{U}$ appearing in (10) depends only on the parameter $\mathscr{M}$. Expressing that relation in dimensional form, we find that the viscosity η for steady-state Coble creep must have the form $\eta = \mu t_d \mathrm{Fn}(\mathscr{M})$. The claim follows.

3. Power series solution

By contrast with the situation for steady creep, for the transient problem, the displacement at the interface is coupled with the stress state within the grain, and the full problem (6) must be solved. We assume the interface position to be given by the Fourier sine series

$$f(x) = \sum_{k=1}^{\infty} f_k \sin kx, \tag{11}$$

where the constants f_k are independent of ε. In particular, for the piecewise linear interface defined by $f(-x) = -f(x)$ and

$$f = \begin{cases} x/\pi\alpha & \text{if } 0<x<\pi\alpha, \\ 1 & \text{if } \pi\alpha<x<\pi(1-\alpha), \\ (\pi-x)/\pi\alpha & \text{if } \pi(1-\alpha)<x<\pi, \end{cases} \tag{12}$$

the Fourier coefficients are given by

$$f_k = 2\{1-(-1)^k\}\frac{\sin k\pi\alpha}{\alpha\pi^2 k^2}, \quad k = 1,2\ldots . \tag{13}$$

If a polycrystal is modelled as a two-dimensional array of regular hexagons, the cases $\alpha = \frac{1}{4}$ and $\alpha = \frac{1}{2}$ correspond to two orthogonal sliding surfaces, called, respectively, 'mode 1' and 'mode 2' surfaces in Raj and Ashby (1971, figure 2.3). We refer to these cases, respectively, as the hexagonal and the sawtooth boundary. We note that because f' is discontinuous at corners for the piecewise linear interface, the corresponding Fourier coefficients decay as k^{-2}.

We now express the solution of the b.v.p. as a power series in the slope parameter ε, so

$$u_i(x,y,t,\varepsilon) = \sum_{k=0}^{\infty} \varepsilon^k u_i^{(k)}(x,y,t), \tag{14a}$$

$$\sigma_{ij}(x,y,t,\varepsilon) = \sum_{k=0}^{\infty} \varepsilon^k \sigma_{ij}^{(k)}(x,y,t), \tag{14b}$$

in particular, $\tau = \tau^{(0)} + \varepsilon\tau^{(1)} + \varepsilon^2\tau^{(2)} + \cdots$. Superscripts in parentheses denote the order in the series. Series (14) holds provided the perturbation displacements are small compared with the imposed displacement U.

To obtain governing equations for the coefficients, we use symbolic manipulation to differentiate the b.v.p. k times with respect to ε, then set $\varepsilon = 0$. To do that, the Cartesian forms of the interfacial conditions (6e)–(6h) are needed. They are given in Appendix A.

3.1. Base state

For $\varepsilon = 0$ the interface is flat, and the governing b.v.p. admits the solution $\boldsymbol{u} = u^{(0)}(y,t)\boldsymbol{e_x}$ describing simple shear. The Navier–Cauchy equation (6b) then requires $\partial^2 u^{(0)}/\partial y^2 = 0$. Condition (6e) of continuity of normal stress is satisfied identically. The corresponding condition (6f) on the shear stress requires $\partial u^{(0)}/\partial y$ to have the same value $\tau^{(0)}(t)$ in each grain. Integrating the expression $\partial u^{(0)}/\partial y = \tau^{(0)}$, then applying the boundary conditions at $|y| = a$, we obtain

$$u^{(0)} = y\tau^{(0)} + \{U - a\tau^{(0)}\}\operatorname{sgn} y. \tag{15}$$

Imposing the slip condition (6h) for $\varepsilon = 0$, we obtain the following differential equation for $\tau^{(0)}(t)$:

$$2a\mathscr{M}\dot{\tau}^{(0)} + \tau^{(0)} = 2\mathscr{M}\dot{U}. \tag{16}$$

We see that the interaction of grain elasticity with slip viscosity causes the sample to behave as a Maxwell solid, at leading order in ε.

Solving (16) for the imposed time-periodic displacement U given by (8a), we find that the stress $\tau^{(0)}$ and slip $[u^{(0)}]$ are given by

$$\tau^{(0)} = \frac{2\mathrm{i}U\omega\mathscr{M}}{1 + 2\mathrm{i}a\omega\mathscr{M}}, \tag{17a}$$

$$[u^{(0)}] = \frac{2U}{1 + 2\mathrm{i}a\omega\mathscr{M}}. \tag{17b}$$

Fig. 2 shows the displacement in the base state. Vanishing slip viscosity η' corresponds to $\mathscr{M} = 0$. According to (17), in that case $\tau^{(0)} = 0$ and $[u^{(0)}] = 2U$. Each grain then slides as rigid unit, the imposed displacement being completely accommodated at the interface. The stress (and the loss spectrum) are then determined at higher order in the perturbation series. That special base state is assumed (implicitly) by Raj and Ashby (1971), and in subsequent papers based on that work. According to (17), even if $\mathscr{M} \neq 0$, their base state occurs if $\omega\mathscr{M} \ll 1$, i.e. if the dimensional frequency $\omega_* \ll t_\eta^{-1}$. (In particular, the analysis in Mosher and Raj, 1974, of elastically accommodated sliding controlled by slip viscosity holds only in that low frequency limit.)

3.2. First-order solution

At $O(\varepsilon)$, the subsidiary conditions are as follows:

$$\text{on } |y| = a, \quad u^{(1)} = 0 = v^{(1)}; \tag{18a,b}$$

$$\text{on } y = 0, \quad \mathscr{M}[\dot{u}^{(1)}] - \sigma_{xy}^{(1)} = 0, \tag{18c}$$

$$[\dot{v}^{(1)}] + \frac{\partial^2 \sigma_{yy}^{(1)}}{\partial x^2} = [\dot{u}^{(0)}]f' + 2\tau^{(0)}f''', \tag{18d}$$

$$[\sigma_{xy}^{(1)}] = 0 = [\sigma_{yy}^{(1)}]. \tag{18e,f}$$

We note that the only inhomogeneous terms occur on the right-hand side (r.h.s.) of the interfacial mass balance (18d). Those terms represent, respectively, the normal component of velocity resulting from the interaction between sliding over topography, and the diffusion of mass that occurs because a normal stress acts on the slightly tilted interface. At points where $\boldsymbol{e_n}$ is discontinuous, the first of those terms causes the singularity discussed in Section 2.1.

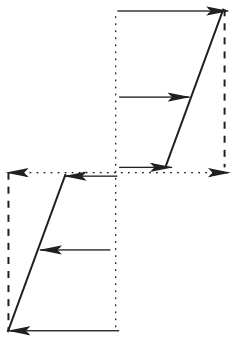

Fig. 2. Displacement in the base state. Broken line, limiting profile for inviscid sliding.

The solution of (18) does not contribute directly to the x-averaged shear stress τ at the sample boundary. The forcing terms in (18d) have zero x-average because the base state is independent of x, and $f(x)$ itself has zero x-mean. Averaging (18) over a wavelength, we find that $\bar{u}^{(1)}=0$. As a result,

$$\tau^{(1)}=0. \tag{19}$$

We must, however, solve (18) since $u^{(1)}$ and $v^{(1)}$ enter into the problem for $\tau^{(2)}$.

For simplicity, we now assume that $a\gg 1$, so the sample thickness is large compared with the fundamental wavelength. With exponentially small error in the large parameter a, conditions (18a) and (18b) at $|y|=a$ can be applied at infinity. (We do not apply the limit $a\to\infty$ to the base state, since (17a) shows that the shear stress τ_0 varies as a^{-1}. So we take exponentially small terms as negligible, but keep terms that are only algebraically small.)

Separating variables, we find that the solution of the Navier–Cauchy equations (6a) and (6b) satisfying (18) is as follows:

$$u^{(1)}=\sum_{k=1}^{\infty}\{2\nu-1+k|y|\}v_k(t)\mathrm{e}^{-k|y|}\sin kx, \tag{20a}$$

$$v^{(1)}=\operatorname{sgn} y\sum_{k=1}^{\infty}\{2-2\nu+k|y|\}v_k(t)\mathrm{e}^{-k|y|}\cos kx, \tag{20b}$$

$$2(1-\nu)\frac{\mathrm{d}v_k}{\mathrm{d}t}+k^3v_k=kf_k\left\{\frac{1}{2}[\dot{u}^{(0)}]-k^2\tau^{(0)}\right\}. \tag{20c}$$

These equations show that $u^{(1)}$ is an even function of y, whereas $v^{(1)}$ is odd. As a result, the shear stress vanishes at the interface, and there is also no slip. At this order, the slip condition (18c) is satisfied identically.

For the stress $\tau^{(0)}$ given by (17a), the time-periodic solution of (20c) is

$$v_k=\frac{1}{2}kf_k\frac{[\dot{u}^{(0)}]-2k^2\tau^{(0)}}{k^3+2\mathrm{i}(1-\nu)\omega}. \tag{21}$$

We note that as $k\to\infty$, $v_k\sim -f_k\tau^{(0)}$, so the Fourier series for $v^{(1)}$ on $y=0^+$ converges at the same rate as the series for interface position $f(x)$. Despite the presence of diffusion in the model, the displacement at the grain interface is no smoother than the imposed topography.

To explain that result, we recall that grain-boundary diffusion is driven by tangential gradients of normal stress. According to Eq. (A.2b), at the interface the normal stress is given by the expression

$$\sigma_{nn}(x,\varepsilon f)=\varepsilon\{\sigma_{yy}^{(1)}-2f'\tau^0\}+O(\varepsilon^2), \tag{22}$$

where the r.h.s. is evaluated at $y=0$. Using (20) to evaluate (22), we obtain

$$\sigma_{yy}^{(1)}=-2\sum_{k=1}^{\infty}kv_k\cos kx, \tag{23}$$

so

$$\sigma_{nn}(x,\varepsilon f,\varepsilon)=-\varepsilon\mathscr{M}^{-1}\tau^{(0)}\sum_{k=1}^{\infty}kf_k\frac{k+4\mathrm{i}(1-\nu)\omega\mathscr{M}}{k^3+2\mathrm{i}(1-\nu)\omega}\cos kx+O(\varepsilon^2). \tag{24}$$

Because the coefficients in this Fourier series for σ_{nn} vary as f_k/k, the series converges more rapidly (by a factor of k) than that for the topography. That behaviour is required by the interfacial mass balance (6g). For example, if $\boldsymbol{e_n}$ is discontinuous, (6g) can be satisfied if $\mathrm{d}^2\sigma_{nn}/\mathrm{d}s^2$ is also discontinuous. But a discontinuity in $\boldsymbol{e_n}$ (e.g. at a corner) requires a discontinuity in f'. As a result, f' and $\mathrm{d}^2\sigma_{nn}/\mathrm{d}s^2$ are equally smooth. So the Fourier coefficients for σ_{nn} must vary as f_k/k, in agreement with (24). Returning now to (22), we see that the l.h.s. is smoother than the second term $2f'\tau^0$ on the r.h.s. As a result, the discontinuity in f' must be cancelled by a corresponding discontinuity in $\sigma_{yy}^{(1)}$. The displacement at the grain interface is therefore no smoother than the topography, as implied by (21). We discuss the physical significance of this result in Section 7.

3.3. Second-order solution

At this order, the subsidiary conditions are as follows:

$$\text{on } |y|=a,\quad u^{(2)}=0=v^{(2)}; \tag{25a,b}$$

on $y=0$,

$$\mathscr{M}[\dot{u}^{(2)}]-\sigma_{xy}^{(2)}=f'\sigma_{yy}^{(1)}-\frac{\partial}{\partial x}(f\sigma_{xx}^{(1)})-\frac{3}{2}f'^2\tau^{(0)}-\mathscr{M}\left\{f\left[\frac{\partial\dot{u}^{(1)}}{\partial y}\right]+f'[\dot{v}^{(1)}]\right\}, \tag{25c}$$

$$[\dot{v}^{(2)}] + \frac{\partial^2 \sigma_{yy}^{(2)}}{\partial x^2} = 0, \tag{25d}$$

$$[\sigma_{xy}^{(2)}] = 0 = [\sigma_{yy}^{(2)}]. \tag{25e,f}$$

To simplify (25d) and (25e) without approximation, we have used the following properties of the first-order solution: $[u^{(1)}] = 0$; $[\partial v^{(1)}/\partial y] = 0$, since $\partial v^{(1)}/\partial y$ is an even function of y; $\sigma_{xy}^{(1)}(x,0) = 0$; and lastly, $[\sigma_{xx}^{(1)}] = 0$. In (25f), we have used the y-component of the equations of equilibrium in the form $\partial\sigma_{xy}/\partial x + \partial\sigma_{yy}/\partial y = 0$; we have also used (18e), i.e. $[\sigma_{xy}^{(1)}] = 0$.

For any function $g(x,y,t)$, 2π-periodic in x but otherwise arbitrary, we define its x-average by

$$\bar{g} = \frac{1}{2\pi}\int_0^{2\pi} g(x,y,t)\,\mathrm{d}x. \tag{26}$$

To determine the resultant force needed to deform the sample, we need solve (25) only for $\bar{u}^{(2)}(y,t)$. Averaging the x-component of the equations of equilibrium, and boundary conditions (25a), (25c), and (25d) we find that $\bar{u}^{(2)}$ satisfies the following b.v.p:

$$\text{within each grain} \quad \frac{\partial^2 \bar{u}^{(2)}}{\partial y^2} = 0; \tag{27a}$$

$$\text{on } |y| = a, \quad \bar{u}^{(2)} = 0; \tag{27b}$$

$$\text{on } y = 0, \quad \left[\frac{\partial \bar{u}^{(2)}}{\partial y}\right] = 0, \tag{27c}$$

$$\mathscr{M}\overline{[\dot{u}^{(2)}]} - \frac{\partial \bar{u}^{(2)}}{\partial y} = \overline{f'\sigma_{yy}^{(1)}} - \frac{3}{2}\overline{f'^2}\tau^{(0)} - 2\mathscr{M}\overline{f'[\dot{v}^{(1)}]}. \tag{27d}$$

The identity

$$\overline{f\left[\frac{\partial u^{(1)}}{\partial y}\right]} = \overline{f'[v^{(1)}]} \tag{28}$$

has been used; it follows from (18e), and the identity $\overline{\partial g/\partial x} = 0$. We do not show the corresponding b.v.p. for $\bar{v}^{(2)}$ since $\bar{v}^{(2)}$ vanishes on the sample boundaries, and so does not contribute to τ.

The solution of (27a) satisfying (27b) and (27c) is

$$\bar{u}^{(2)} = (y - a\,\mathrm{sgn}\,y)\tau^{(2)}. \tag{29}$$

Substituting (29) into (27d), we obtain the following differential equation for $\tau^{(2)}(t)$:

$$2a\mathscr{M}\dot{\tau}^{(2)} + \tau^{(2)} = \frac{3}{2}\overline{f'^2}\tau^{(0)} - \overline{f'\sigma_{yy}^{(1)}} + 2\mathscr{M}\overline{[\dot{v}^{(1)}]f'}. \tag{30}$$

Eq. (30) expresses the balance of forces acting in the x-direction on the upper elastic layer, as we now discuss. Since the discontinuity in $u^{(2)}$ across the interface is given by $-2a\tau^{(2)}$, the first term on the l.h.s. of (30) describes the stress that would be exerted on the upper layer by a plane viscous interface. That stress and the boundary stress $\tau^{(2)}$ together balance the resultant stress represented by three terms on the r.h.s. of (30). Those terms have the following interpretation. The first represents the interaction of the base shear stress $\tau^{(0)}$ with the increased interfacial area created by topography; and the second and third terms represent, respectively, the x-components of σ_{nn} and σ_{ns}.

4. General solution for G

Using (20b) and (23) to evaluate the r.h.s. of (30), we find that

$$2a\mathscr{M}\dot{\tau}^{(2)} + \tau^{(2)} = \sum_{k=1}^{\infty} k^2 f_k \left\{(1 - 2k^2\mathscr{M})v_k + \left(\frac{7}{4} - 2k^2\mathscr{M}\right)f_k\tau^{(0)}\right\}.$$

Substituting for $\tau^{(0)}$ and v_k from (17a) and (21), then solving for the time-periodic stress $\tau^{(2)}$, we obtain

$$(1 + 2\mathrm{i}a\mathscr{M}\omega)^2\tau^{(2)} = \mathrm{i}\omega U\sum_{k=1}^{\infty} k^2 f_k^2 \frac{\mathrm{i}\omega\mathscr{M}(1-\nu)(7 - 8k^2\mathscr{M}) + k - \frac{1}{2}k^3\mathscr{M}}{2\mathrm{i}(1-\nu)\omega + k^3}. \tag{31}$$

(The coefficients f_k are given by Eq. (13).) Using (14b) and (8c), we find that

$$\tau = \tau^{(0)} + \varepsilon^2\tau^{(2)} + O(\varepsilon^4), \tag{32}$$

$$G = a(\tau^{(0)} + \varepsilon^2\tau^{(2)})/U. \tag{33}$$

This solution holds if the displacement perturbations are small compared with those in the base state. In that state, the displacement is $O(U)$, whereas the mean second-order displacement is $O(\varepsilon^2 a|\tau^{(2)}|)$, by (29). Because the ratio of those displacements is $O(\varepsilon^2 a|\tau^{(2)}|/U)$, the solution is valid if

$$\varepsilon^2|G^{(2)}| \ll 1, \tag{34}$$

i.e. if the perturbation to the sample rigidity G is small compared with the unit rigidity of the individual elastic layers. To avoid misunderstanding, we note that because (34) does not restrict $G^{(0)}$, it does not require G itself to be close to unity; though a sample comprising two elastic layers separated by a plane inviscid interface has $G = 0$, it is evidently described by our solution. Eq. (34) is satisfied for all examples given below.

5. Significance of the separation of timescales for $\mathscr{M} \ll 1$

Fig. 3 shows the sample rigidity G as a function of angular frequency. All curves were computed using $N = 100$ terms of series (11) defining the interface shape; with the exception of that for $\mathscr{M} = 10^{-9}$, all are graphically identical for $N = 10, 100$. In Fig. 3a, the important feature is that if $\mathscr{M} \sim 1$, so the viscous timescale $t_v \sim t_d$, the mechanical loss $\mathscr{L}$ varies roughly as ω^{-1}.

To explain that result, we note that the slip condition (6h) requires that if $\mathscr{M} \sim 1$, the slip $[u_s] \to 0$ for $\omega \gg 1$. Without slip, the sample is in pure shear. Though it is obvious that slip viscosity then does not cause attenuation, a more careful argument is needed for diffusion. The diffusive mass flow along the interface is driven by tangential gradients of normal stress. But in a state of pure uniform shear, σ_{nn} is uniform along any linear portion of the interface. As a result, the diffusive flux vanishes except near corners, where σ_{nn} changes from one uniform value to another. According to Eq. (4), the dimension ℓ_d on which diffusion modifies such a nearly discontinuous stress vanishes for $\omega \gg 1$. Consequently, diffusion

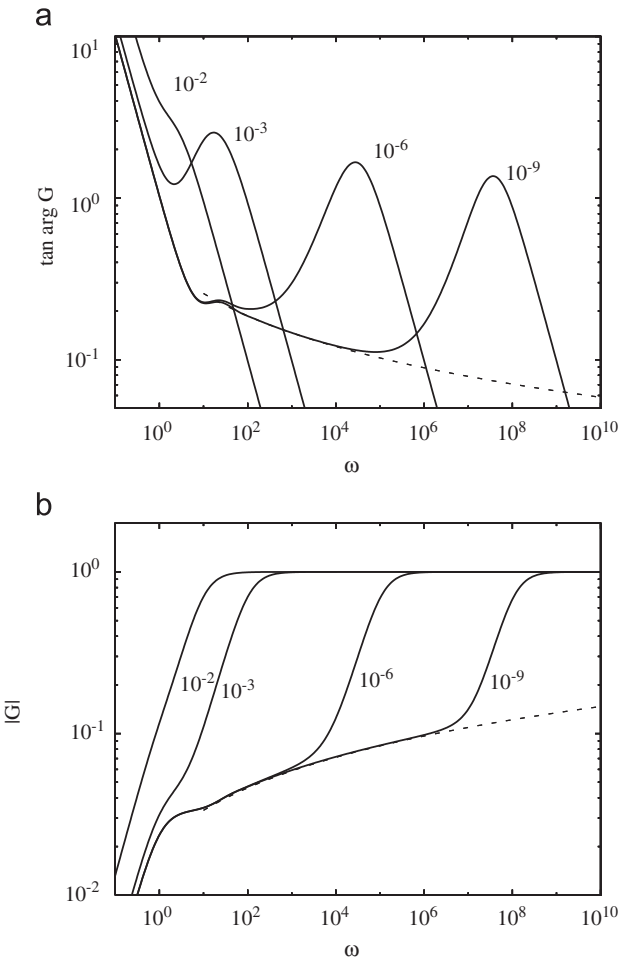

Fig. 3. Sliding with concurrent diffusion and slip viscosity: sample rigidity G computed from (33) for a sawtooth interface with $N = 100$. Parameters: $\alpha = \frac{1}{2}$, sample thickness $2a = 10$, Poisson ratio $\nu = \frac{1}{2}$ and $\varepsilon^2 = 0.01$. Curve labels: Maxwell ratio $\mathscr{M}$. Broken curve, Eq. (38b). As in the text, angular frequency ω is expressed in diffusion units t_d.

operates over a vanishingly small fraction of a wavelength. We conclude that for $\mathscr{M}\sim 1$, the diffusional contribution to $\mathscr{L}$ is vanishingly small for $\omega \gg 1$. Because neither attenuation mechanism is effective, $\mathscr{L}$ decreases rapidly with increasing frequency when $\mathscr{M}\sim 1$.

That explanation is consistent with another feature of Fig. 3a. As shown by the curve for $\mathscr{M} = 10^{-9}$, when $\mathscr{M} \ll 1$, so the relaxation times are widely separated, there is wide range of ω within which $\mathscr{L}$ decreases only slowly. The slipcondition (6h) now requires $[u_s] \to 0$ only when $\omega\sim\mathscr{M}^{-1}$. As a result, there is a band of frequencies, namely $1 \ll \omega \ll \mathscr{M}^{-1}$ within which the sample is *not* in a state of pure shear. Slow attenuation therefore occurs by diffusion over large distances, even at very high frequencies. (That mechanism for slow attenuation is discussed further in the following section.) Attenuation ceases only when the interface becomes welded at frequencies large compared with $\mathscr{M}^{-1}$. That cut-off is preceded by a local maximum in mechanical loss due to the slip viscosity as discussed in the context of Fig. 4. We conclude that $\mathscr{M} \ll 1$ is a necessary condition for a range of frequencies to exist within which $\mathscr{L}$ can vary slowly with ω. According to this analysis, when such a region is observed in the loss spectrum of finely grained sample in which the only dissipative mechanisms are grain-boundary diffusion and a slip viscosity, the timescales must be widely separated, i.e. $\mathscr{M} \ll 1$. This conclusion should be insensitive to model detail, because it results from the general form of boundary conditions (6g) and (6h).

In Fig. 3b, the important feature is that $|G| \leqslant 1$. As noted in Section 1, allowing slip along the interface cannot increase the sample rigidity over its unit value for the individual grains. As $\omega \to \infty$, $|G| \to 1$ because the slip condition (6h) requires that $[u_s] \to 0$ at high frequency, independent of interface geometry. As noted in the discussion of Eq. (34), although $|G| \to 0$ as $\omega \to 0$ the results shown in this figure are in fact compatible with that condition for the validity of the perturbation method.

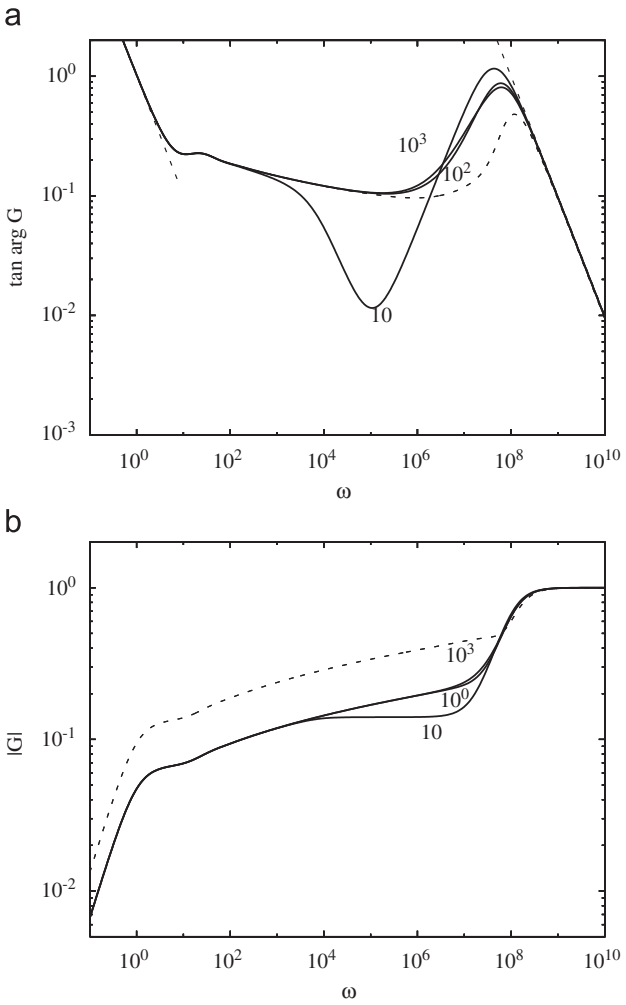

Fig. 4. Sliding on a 'hexagonal' interface with concurrent diffusion and slip viscosity: effect of varying N on G. Maxwell ratio $\mathscr{M} = 10^{-9}$; for that value, the sliding frequency t_d/t_v occurs at $\omega = 10^9$. Curve labels give the value of N; for other parameters, see Fig. 3. Solid curves, $\varepsilon^2 = 0.01$. Broken curve, $\varepsilon^2 = 0.02$ and $N = 10^3$; broken lines, Eq. (38a), and a high-frequency asymptote obtained from (17).

Fig. 4shows the effect on G of varying the number N of terms used in the Fourier series representation of the 'hexagonal' interface obtained by setting $\alpha = \frac{1}{4}$ in (12). For $N \to \infty$, the slope is discontinuous at corners and, as discussed above (8), that discontinuity in $\boldsymbol{e_n}$ would cause a corresponding discontinuity in $\boldsymbol{u}$ if diffusion were absent. For finite N that discontinuity is smoothed over a distance $\sim N^{-1}$. Faul et al. (2004) suggest that effect may determine whether a local maximum due to the slip viscosity is observable over a background spectrum. To some extent, that suggestion is supported by Fig. 4a. But although reducing N does increase the height of the maximum, the effect is weak, and is further constrained because N is bounded. For grain size d, and corner length r_c, $N < d/r_c$, so that for $d = 1\,\mu\text{m}$ and $r_c = 1\,\text{nm}$, $N < 10^3$. The figure shows that reducing N from 10^3 to 10 increases the maximum by only ~30%. The corresponding frequency also varies only weakly with N. Numerical solutions for finite ε confirm that smoothing the corners has only a modest effect on the local maximum due to the slip viscosity (Lee et al., 2007).

6. Inviscid sliding

We have seen that to obtain a band of frequency within which $\mathscr{L}$ can vary slowly with ω, it is necessary that $\mathscr{M} \to 0$, so there is a separation of timescales. To study the form of $\mathscr{L}$ within that frequency band, we now take $\mathscr{M} = 0$ in our general solution. In the base state described by (17), $[u^{(0)}] = 2U$, so that the imposed displacement is accommodated by slip and the individual grains are in rigid-body translation.

6.1. Fourier transform

Because $\tau^0 = 0 = \tau^{(1)}$, the x-averaged stress τ is given by $\varepsilon^2\tau^2 + O(\varepsilon^4)$. We let

$$\tilde{\omega} = 2(1-\nu)\omega, \tag{35}$$

so that $\tilde{\omega}$ is the dimensional angular frequency ω_* measured in units $t_d/2(1-\nu)$. (This modified timescale is identical with that defined by Eq. (10) of Raj, 1975.) From (32) with $\mathscr{M} = 0$, we obtain

$$\tau = 2\varepsilon^2 \frac{U}{1-\nu} g(\tilde{\omega}), \tag{36a}$$

$$g(\tilde{\omega}) = \frac{1}{4}\mathrm{i}\tilde{\omega} \sum_{k=1}^{\infty} \frac{k^3 f_k^2}{\mathrm{i}\tilde{\omega} + k^3}; \tag{36b}$$

$$\mathscr{L} = \tan \arg g \tag{36c}$$

because G/g is real. We note that Eq. (36c) gives the limit as $\varepsilon \to 0$ of the mechanical loss. Although the result for $\mathscr{L}$ is independent of ε, that is a consequence of its being a limiting value. (In Section 7, we explain physically why $\mathscr{L}$ must depend on ε.)

For the sawtooth interface ($\alpha = \frac{1}{2}$), and $f_{2k+1} = 8(-1)^k/\pi^2(2k+1)^2$ and $f_{2k} = 0$ by (12). So

$$g(\tilde{\omega}) = \frac{16}{\pi^4}\mathrm{i}\tilde{\omega} \sum_{k=0}^{\infty} \frac{1}{(2k+1)\{(2k+1)^3 + \mathrm{i}\tilde{\omega}\}}. \tag{37}$$

For the hexagonal interface ($\alpha = \frac{1}{4}$), $g(\tilde{\omega})$ has exactly twice the value given by (37). Because that factor is real, $\mathscr{L}$ is the same for both cases.

We state the asymptotes for g; they are interpreted physically in Section 7. Letting $c = 127\zeta(7)/8\pi^4 \doteq 0.164$, where $\zeta(n)$ is the Riemann zeta function, we have

$$g = \tfrac{1}{6}\mathrm{i}\tilde{\omega} + c\tilde{\omega}^2 + O(\tilde{\omega}^3) \quad \text{for } \tilde{\omega} \to 0; \tag{38a}$$

$$g = \frac{8}{3\pi^4}\{\ln(8\mathrm{i}\tilde{\omega}) + 3\gamma_E\} + o(1) \quad \text{for } \tilde{\omega} \to \infty. \tag{38b}$$

Here, $\gamma_E \doteq 0.577$ denotes the Euler constant, and we use standard order notation; in the limit specified, $f = O(g)$ implies that f/g approaches a non-zero constant, whereas $f = o(g)$ implies that $f/g \to 0$. Eqs. (38a) and (38b) hold only for the sawtooth interface; corresponding results for the hexagonal interface are obtained by doubling the value given by (38).

Because (38b) is used immediately below, and again in the next section on the creep function, we note that it is obtained by a standard method. The Cauchy residue theorem is applied to the function $\psi(z)/(1-2z)\{(1-2z)^3 + \mathrm{i}\tilde{\omega}\}$, where ψ is the Euler psi function. The contour is a circle of infinite radius centred on the origin of the complex z plane. We also note that result (38b) of this procedure is consistent with Eq. (34). According to that condition, the solution holds if $2\varepsilon^2 a|g|/(1-\nu) \ll 1$. For any finite value of $\tilde{\omega}$, no matter how large, (38b) satisfies that criterion if ε is sufficiently small.

The corresponding expressions for the mechanical loss are

$$\mathscr{L} = \begin{cases} 1/6c\tilde{\omega} & \text{for } \tilde{\omega} \to 0, \\ \pi/2(\ln 8\tilde{\omega} + 3\gamma_E) & \text{for } \tilde{\omega} \to \infty. \end{cases} \tag{39a,b}$$

According to (39), $\mathscr{L}$ varies inversely with frequency at low frequencies, but varies inversely with $\ln\tilde{\omega}$ at high frequencies. We note that Eq. (39b) differs from a result given by Gribb and Cooper (1998); without proof, they state that small-slope analysis of the Raj–Ashby model requires $\mathscr{L}\sim\omega^{-1/2}$ at high frequencies. Using the next figure, we show that the asymptotes given by (39) agree with the result obtained by evaluating (37) numerically.

Fig. 5 shows the scaled rigidity g calculated as a function of angular frequency. Comparing the l.h.s. and r.h.s. of the curve for $N=10$ terms of sum (37), we see that the loss spectrum consists of two regions in which $\mathscr{L}$ decreases rapidly (as $\tilde{\omega}^{-1}$), separated by an extensive range of frequency within which $\mathscr{L}$ decreases slowly, in agreement with Eq. (39b). The solid curve for 100 terms is similar, except that $\mathscr{L}$ now follows Eq. (39b) over a wider range of frequency. The behaviour for $|g|$ is similar: for moderately high frequencies, $|g|$ follows asymptote (38b), but at very high frequencies, the curve for 10 terms shows that $|g|$ approaches a limit whose value depends on the number of terms used to approximate the sum. (We note that, according to Fig. 3a, the general (viscous) solution also obeys Eq. (39a,b) for $1\ll\tilde{\omega}\ll\mathscr{M}^{-1}$.)

The present figure also includes two other asymptotes showing the effect of truncating the Fourier series at N terms. (To avoid clutter, these asymptotes are shown for only two of the curves.) Rewriting the partial sum of N terms of (37), we obtain without approximation

$$\frac{\pi^4}{16}g_N(z)=\sum_{k=0}^{N-1}\frac{1}{(2k+1)\{1-\mathrm{i}(2k+1)^3/\tilde{\omega}\}}, \tag{40a}$$

$$=\frac{1}{2}\{\ln 4N+\gamma_E\}+\frac{4}{3}\mathrm{i}N^3\tilde{\omega}^{-1}+O(\tilde{\omega}^{-2}). \tag{40b}$$

To obtain (40b), the binomial theorem has been used, together with some standard summations. According to (40b), as $\tilde{\omega}/N^3\to\infty$,

$$|g_N|=\frac{8}{\pi^4}\{\ln 4N+\gamma_E\}+o(1), \tag{41a}$$

$$\tan\arg g_N=\frac{8}{3}\frac{N^3}{\ln 4N+\gamma_E}\tilde{\omega}^{-1}+O(\tilde{\omega}^{-2}). \tag{41b}$$

Rounding the corners over a horizontal scale $\sim N^{-1}$ thus affects the rigidity at frequencies $>N^3$. At lower frequencies, diffusion relaxes the stress singularity, and the details of the corner have no effect on $\mathscr{L}$. Eq. (41) also shows that for $\tilde{\omega}/N^3\to\infty$, $|g_N|$ approaches a limit, but the magnitude of that limit itself increases with N. The mechanical loss now varies inversely with frequency. That behaviour is explained physically in Section 7.

To relate our solution to that of Raj (1975), we now use our solution for the Fourier transform of the stress to obtain the creep function, i.e. the response in time of the sample to a Heaviside step in stress.

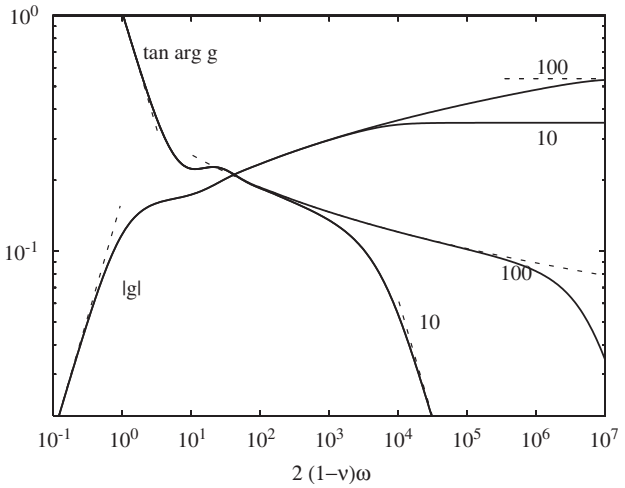

Fig. 5. Inviscid sliding on a sawtooth boundary: scaled rigidity g calculated from (37) for the values of N given in the curve labels. Broken curves, Eqs. (39) and (41).

6.2. Creep function

Letting $U = \hat{U}(\omega)e^{i\omega t}$ and $\tau = \hat{\tau}(\omega)e^{i\omega t}$ in (36), and also letting

$$S(i\tilde{\omega}) = \sum_{k=0}^{\infty} \frac{1}{(2k+1)\{(2k+1)^3 + i\tilde{\omega}\}}, \tag{42}$$

we find that the transform $\hat{U}$ of the boundary displacement caused by arbitrary applied stress $\tau(t)$ is given by

$$\frac{64\varepsilon^2}{\pi^4}\hat{U}(\omega) = \frac{\hat{\tau}(\omega)}{i\omega S(i\tilde{\omega})}. \tag{43}$$

Letting $\tau(t)$ be the unit impulse (Dirac delta) function, so that $\hat{\tau} = 1$, we see that to within a constant factor, the function $1/i\omega S$ is the Fourier transform of the boundary displacement caused by a unit stress impulse.

Using that interpretation, we locate the singularities of $\hat{U}$ in the complex ω plane. Because the sample behaves as a viscous fluid on long timescales, as $t \to \infty$ the boundary displacement caused by a stress $\delta(t)$ must approach a limit determined by the pole of $1/i\omega S$ at the origin. As no physical mechanism exists to drive oscillations in this over-damped system, that limiting displacement must be approached monotonically in t. All other poles of $1/i\omega S$ therefore lie along the positive imaginary ω axis.

With those properties of $\hat{U}$ established, we determine the displacement $U(t)$ corresponding to a Heaviside unit step in applied stress. For $\mathrm{Im}\,\omega < 0$, $\hat{\tau}$ is then defined by the integral

$$\hat{\tau} = \int_0^{\infty} e^{-i\omega t} dt = \frac{1}{i\omega}. \tag{44a,b}$$

Though integral (44a) defines $\hat{\tau}$ only in the lower half ω-plane, by analytic continuation, the second equation (44b) gives the transform uniquely in the whole plane. The transform $\hat{U}$ of the creep function thus has a double pole at the origin, and poles elsewhere along the positive imaginary axis.

Using the Fourier inversion theorem in the form stated by Davies (1985, p. 90), we find the creep function $U(t)$ to be given by the expression

$$\frac{64\varepsilon^2}{\pi^4}U(t) = \frac{1-\nu}{\pi}\int_{-\infty-ci}^{\infty-ci} \frac{e^{i\tilde{\omega}t/2(1-\nu)}d\tilde{\omega}}{(i\tilde{\omega})^2 S(i\tilde{\omega})}. \tag{45}$$

The arbitrary constant $c > 0$, so the inversion contour passes below the pole of the integrand occurring at $\tilde{\omega} = 0$.

Letting $p = i\tilde{\omega}$, we rewrite (45) in the form of the inversion integral for the Laplace transform:

$$\frac{64\varepsilon^2}{\pi^4}U(t) = \frac{1-\nu}{\pi i}\int_{c-i\infty}^{c+i\infty} \frac{e^{pt/2(1-\nu)}dp}{p^2 S(p)}. \tag{46}$$

In the p-plane, the corresponding poles are along the negative real axis. Using standard theory, we may express that integral in terms of the sum of the residues at poles of the integrand:

$$\frac{1}{2\pi i}\int_{c-i\infty}^{c+i\infty} \frac{e^{pt/2(1-\nu)}dp}{p^2 S(p)} = S_0^{-1}\left\{\frac{t}{2(1-\nu)} - \frac{S_0'}{S_0}\right\} + \sum_{i=1}^{\infty} \frac{e^{p_i t/2(1-\nu)}}{p_i^2 S'(p_i)}. \tag{47}$$

$S_0 = 1.015\ldots$, $S_0' = -1.000\ldots$. The first term in braces accounts for the double pole at the origin. In the second term, the infinite sum extends over all zeros p_i of the function $S(p)$; that term accounts for residues at the simple poles of the integrand on the negative real p axis. According to Table 1, both p_i and $S'(p_i)$ are negative, so the infinite sum increases

Table 1
Constants used to evaluate Eq. (49).

i	$-p_i$	$-S'(p_i)$
1	20.2392	0.100141×10^{-1}
2	108.8488	0.905406×10^{-3}
3	314.1395	0.192112×10^{-3}
4	684.3126	0.606853×10^{-4}
5	1267.503	0.242032×10^{-4}
6	2111.811	0.112578×10^{-4}
7	3265.315	0.584117×10^{-5}
8	4776.078	0.328883×10^{-5}
9	6692.155	0.197311×10^{-5}
10	9061.59	0.124539×10^{-5}
11	11932.4	0.819388×10^{-6}

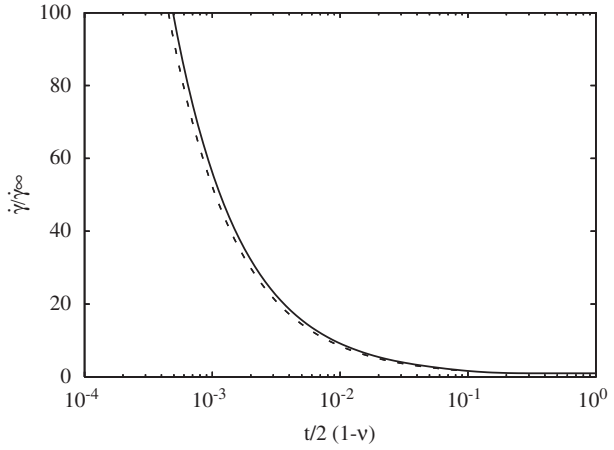

Fig. 6. Inviscid sliding on a sawtooth boundary: creep rate $\dot{\gamma}=\dot{U}/a$ normalized against its steady-state value as a function of $t/2(1-\nu)$; dimensionless time is given in diffusion units ($t=t_*/t_d$). Solid curve, Eq. (49); broken curve, Eq. (50b) normalized against the steady-state creep rate.

monotonically from its initially negative value, and ultimately vanishes. Physically, the first term represents the ultimate state in which the boundary creeps with constant velocity; and the second represents the effect of transient creep.

The steady creep rate $\dot{U}_\infty$ is given by

$$\frac{64\varepsilon^2}{\pi^4}\dot{U}_\infty \sim S_0^{-1}. \tag{48}$$

(A similar expression is given as Eq. (23) of Raj and Ashby, 1971.) According to (48), the steady creep rate is independent of Poisson ratio ν. That is to be expected since at low frequencies, the imposed displacement is accommodated by diffusion, allowing the individual grains to respond as rigid bodies.

For arbitrary times, the creep velocity is given by

$$\dot{U}/\dot{U}_\infty = 1 + S_0 \sum_{i=1}^{\infty} \frac{e^{p_i t/2(1-\nu)}}{p_i S'(p_i)}. \tag{49}$$

This simple explicit form is new; both Raj (1975) and Gribb and Cooper (1998) give the creep function in graphical form.

Fig. 6 shows the creep rate $\dot{\gamma}=\dot{U}/a$ calculated from (49), and the numerical values given in Table 1. Those values were obtained using 801 terms in series (42) defining $S(p)$; varying the number of terms does not change the values of p_i and $S'(p_i)$ quoted in the table. Sum (49) was approximated by its first 11 terms; at a value $t=0.0005$ even smaller that those illustrated, the 11th term contributes only about 0.2% to the sum.

We predict higher creep rates than do either Raj (1975) or Gribb and Cooper (1998). That is consistent with our equation (38b) which shows that the Fourier transform decays more slowly with frequency than predicted by Gribb and Cooper (1998). As a check on the numerical evaluation of (49), we also show as a broken curve the small-t asymptote given as Eq. (50b). From the figure, it may not be apparent that the solid curve is in fact asymptotic as $t\to 0$ to the broken curve. On one hand, the curves intersect near $t=0.1$; on the other, the curves converge only very slowly as $t\to 0$. As we shall see, that effect occurs because the asymptotic series is an expansion in powers of $1/|\ln t|$, so t must be extremely small for the asymptotic nature of the series to be graphically evident. Despite that, the figure shows that the first term in the asymptotic series gives a good approximation to the creep curve for $t<0.1$.

To obtain that asymptote, we use the Heaviside series expansion(Davies, 1985, p. 86); i.e. we obtain an asymptotic expansion for $p\to\infty$ of the integrand in (46), then invert termwise. Using the high-frequency asymptote for $S(p)$ obtained from Eq. (38b), we find that

$$\frac{1}{p^2 S(2(1-\nu)p)} \sim \frac{12(1-\nu)}{p\ln(p/\kappa)}, \tag{50a}$$

$$\kappa^{-1} = 16(1-\nu)e^{3\gamma_E}. \tag{50b}$$

Without further approximation, we find that $64\varepsilon^2 U(t)/\pi^4 \sim 12(1-\nu)\phi(\kappa t)$,

$$\phi(t) = \int_0^\infty \frac{t^\xi}{\xi!}\mathrm{d}\xi.$$

(We have used the fact that the Laplace transform of $\phi(t)$ is $1/p\ln p$.) Finally, noting that for $t\leqslant 1$, $t^\xi = e^{-\xi|\ln t|}$, we use Laplace's method to evaluate $\phi(t)$ for $t\to 0$. The displacement U caused by a Heaviside unit step in stress is thus given

for $t \to 0$ by

$$\frac{64\varepsilon^2}{\pi^4} U(t) \sim -\frac{6}{\ln \kappa t}. \tag{50b}$$

According to this equation, as $t \to 0$, the boundary displacement vanishes, but the velocity $\dot{U} \to \infty$. That behaviour is the expression in the time domain of an equivalent singularity in the frequency domain. As we note below Eq. (38), for vanishing slip viscosity η' the perturbation series breaks down at very high frequencies; in the time domain, that corresponds to (50b) breaking down during a short initial period, the length of which vanishes as $\varepsilon \to 0$.

7. Interpretation using energetics

Dimensional variables are now used without asterisks. As shown in Appendix B, for the (two-grain) system shown in Fig. 1, the external power supplied at the sample boundaries by the x-averaged shear stress τ is either dissipated at the time-independent grain interface $\mathscr{S}_I$, or stored as strain energy within the perfectly elastic grains, i.e.

$$2\lambda\tau \frac{\mathrm{d}U}{\mathrm{d}t} = \Upsilon + \frac{\mathrm{d}W}{\mathrm{d}t}, \tag{52a}$$

$$\Upsilon = \int_{\mathscr{S}_I} \left\{ \frac{V\ell D}{kT} \left(\frac{\mathrm{d}\sigma_{nn}}{\mathrm{d}s} \right)^2 + \frac{\ell}{\eta'} \sigma_{ns}^2 \right\} \mathrm{d}s, \tag{52b}$$

$$W = \mu \int_{\mathscr{V}} \left\{ \frac{\nu}{1-2\nu} \theta^2 + e_{ij}^2 \right\} \mathrm{d}\mathscr{V} \tag{52c}$$

define the dissipation function Υ and the strain energy function W. In (52c), $\mathscr{V}$ is the combined, time-independent volume of the upper and lower grains, but with the dissipative interfacial region excluded. Eq. (52) holds for arbitrary interface slope. In Eq. (52a), $\lambda = 2\pi/\xi$ is the wavelength of the interface topography.

Using Eq. (52), we explain the chief features of the loss spectrum for a sawtooth interface. For simplicity, we assume the sample thickness and wavelength to be comparable, and of order d; we also set the slip viscosity $\eta' = 0$. Dissipation thus occurs by grain-boundary diffusion alone. The following arguments are based on the interpretation of $\mathscr{L}$ as the ratio of the power dissipated per cycle to the mean strain energy stored within the sample: i.e. $\mathscr{L} \sim \Upsilon/\omega W$.

First, let us consider the behaviour at low frequency, i.e. for $\omega t_d \to 0$. In that limit, the stress varies smoothly along the grain interface (see Raj, 1975, for the present model; and Ford et al., 2004, for polycrystals). As a result, $W \sim \sigma_{nn}^2 d^2/\mu$, where σ_{nn} is a characteristic normal stress on the grain interface. Further, because σ_{nn} varies smoothly along the interface, $\mathrm{d}\sigma_{nn}/\mathrm{d}s \sim \sigma_{nn}/d$, so that $\Upsilon \sim VD\ell\sigma_{nn}^2/kTd$. Using definition (3b) of t_d, we find that for $\omega t_d \to 0$

$$\mathscr{L} \sim 1/\omega t_d; \tag{53}$$

because the stress field is now independent of ω, the energy dissipated per oscillation is proportional to the oscillation period. Eq. (39a) gives the corresponding quantitative expression.

In the other extreme, $\omega t_d \gg 1$. At those frequencies, the diffusion length $\ell_d \ll d$ so there is a separation of length scales. We consider the deformation at distances r from a corner O of the interface, such that $\ell_d \ll r \ll d$. The first inequality implies that boundary condition (6g) can be approximated by $[\boldsymbol{u} \cdot \boldsymbol{e_n}] = 0$. We develop that equation for a corner subtending an angle close to π, so the interface slope is small. As a first approximation, we may then take the elastic layers to be individually in rigid translation, so the sample deforms only by slip. To obtain the next approximation, we write the displacement in the form $\boldsymbol{u} = \pm U\boldsymbol{e_x} + \boldsymbol{u}'$ where $|\boldsymbol{u}'| \ll U$. Substituting for $\boldsymbol{u}$ in the condition $[\boldsymbol{u} \cdot \boldsymbol{e_n}] = 0$, we obtain $[u_n'] = -2U\boldsymbol{e_n} \cdot \boldsymbol{e_x}$.

Fig. 7 summarizes this picture. On ray OA, $[u_n'] > 0$, and uniform, as depicted by the double arrows, and similarly on ray OB, $[u_n'] < 0$. The resulting stress field is exactly that resulting from the insertion of a slice of matter along ray OA, and the removal of an identical slice along ray OB. That stress field can be obtained by superposing stresses due to two edge dislocations with Burgers vectors normal to the rays OA and OB. The corresponding stress tensor

$$\sigma_{nn} \sim \varepsilon\mu U/r, \tag{54}$$

as could also be obtained by dimensional analysis.

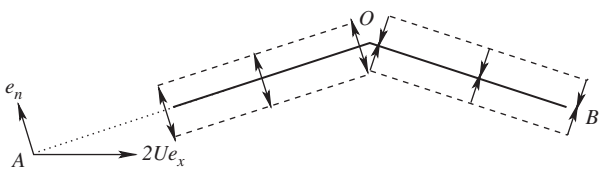

Fig. 7. Interpretation of the high-frequency asymptote.

Using (54) to estimate the strain energy and dissipation functions, we find that

$$W \sim \mu\varepsilon^2 U^2 \ln\frac{d}{\ell_d}, \tag{55a}$$

$$\Upsilon \sim \int_{\ell_d}^{d} \frac{V\ell D}{kT}\left(\frac{\mathrm{d}\sigma_{nn}}{\mathrm{d}r}\right)^2 \mathrm{d}r \sim \mu\varepsilon^2 \frac{d^3U^2}{t_d\ell_d^3}. \tag{55b}$$

(We have used the definition of t_d in the form $V\ell D/kT \sim d^3/\mu t_d$.) Together, the two members of (55) require that for $\omega t_d \gg 1$,

$$\mathscr{L} \sim \frac{d^3}{\omega t_d \ell_d^3 \ln(d/\ell_d)}. \tag{55b}$$

Because we have not yet introduced a specific form ℓ_d, we can use Eq. (55b) to explain the various high-frequency asymptotes included in Fig. 5.

There are two cases. First, the cut-off length can be set by diffusion. In that case, Eqs. (3) and (4) together require that $(d/\ell_d)^3 \sim \omega t_d$. Substituting that expression into (55b), we find that for $\omega t_d \gg 1$,

$$\mathscr{L} \sim 1/\ln(\omega t_d). \tag{57}$$

The mechanical loss therefore varies with $\ln\omega$ at high frequencies, if the corners are infinitely sharp. This explains the form of the quantitative result given as Eq. (39).

Secondly, the corner can be rounded at a length scale that is independent of ω. In the computed solution discussed in Section 6 that occurs because the Fourier series for the interface is truncated at N terms; the corner length scale is then $\sim d/N$. (Faul et al., 2004 argue that this effect has been realized in experiments in which it a second phase is present on the grain boundaries.) When that second length scale is present, the cut-off scale is given by the larger of the diffusion length and d/N. As a result, (55b) requires that if $\omega t_d \gg N^3$,

$$\mathscr{L} \sim \frac{N^3}{\omega t_d \ln N}. \tag{58}$$

(For $1 \ll \omega t_d \ll N^3$, Eq. (57) continues to hold.) This explains the form of the quantitative result given as Eq. (41).

We note that for diffusionally accommodated grain sliding, rounding the corners actually reduces the mechanical loss at sufficiently high frequencies. According to the scaling argument, that reduction occurs because integral (55b) determining $\Upsilon$is asymptotically determined by the length scale d/N. As a result, the integral is asymptotically independent of ω, and the loss per cycle is then proportional to oscillation period, as expressed by (58).

Together, (57) and (58) explain the forms of the quantitative high-frequency asymptotes derived in Section 6. These scaling arguments hold only for small slopes; only then can $\boldsymbol{u}$ be decomposed into a known base state, and a small perturbation. According to Picu and Gupta (1996), local analysis for arbitrary slope shows that the stress singularity at a corner weakens with increasing slope. The implications of that weakened singularity for the loss spectrum will be considered in a subsequent paper.

8. Summary and conclusions

The role of grain-boundary sliding in the viscoelastic relaxation of polycrystalline materials has been revisited through the construction and solution of the boundary value problem (b.v.p.) describing sliding, both elastically and diffusionally accommodated, on a corrugated interface. The grains are modelled by perfectly elastic layers of finite thickness, Poisson ratio ν and rigidity μ. Those layers are separated by a time-independent, spatially periodic interface of fundamental wavelength $2\pi/\xi$ and effective thickness ℓ. Mechanical energy is dissipated solely on the interface by grain-boundary diffusion and viscous slip; the grain-boundary diffusivity and slip viscosity are, respectively, denoted by D and η'. Because there are two dissipative processes, our model contains the two timescales defined by (3), namely $t_\mathrm{v} = \eta'/\ell\mu\xi$ and $t_d = kT/\mu V\ell D\xi^3$, where V, k are the molecular volume and Boltzmann constant (Mosher and Raj, 1974; Raj, 1975). The scales t_v and t_d are the characteristic times taken for an initial stress distribution to equilibrate if viscous slip and diffusion, respectively, act alone. Assuming small interface slope parameter ε, we derive a perturbation solution for the complete mechanical relaxation spectrum. The solution is initially derived and interpreted for arbitrary values of the control parameter $\mathscr{M} = t_\mathrm{v}/t_d$. Guided by experimental observations of attenuation in polycrystals, we then stress the case $\mathscr{M} \ll 1$, in which the timescales are widely separated. In that extreme, the loss spectrum shows the following features.

(a) At high frequencies $\omega > 1/t_\mathrm{v}$, the mechanical loss $\mathscr{L}$ decreases strongly with increasing frequency ($\mathscr{L} \sim 1/\omega$) and the effective shear modulus G approaches the unrelaxed elastic modulus μ.
(b) With decreasing frequency, a Debye-like dissipation peak forms at $\omega \sim 1/100t_\mathrm{v}$. That maximum is associated with a marked reduction of the shear modulus, and is caused by elastically accommodated grain-boundary sliding. Though, in the small-slope regime studied here, the peak height varies significantly with interfacial slope, it varies only weakly as the grain corners are rounded.

(c) With further decrease of frequency towards $1/t_d$, diffusion becomes progressively more effective in smoothing stress concentrations at relatively sharp grain corners ($N \geqslant 10^2$). This regime ($1/1000t_v > \omega > 10/t_d$) is characterized by the very mild variation of mechanical loss (and modulus) with frequency and grainsize described by Eq. (39). (The corresponding result for the creep function is given by Eq. (50b).) According to the physical arguments given in Section 7, those results are consequences of stress singularities near corners and using the local analysis of Picu and Gupta (1996) suggests that the detailed form of the loss spectrum is likely to depend on interface slope.

(d) Within that regime, in which $1/1000t_v > \omega > 10/t_d$, substantial rounding of grain corners ($N \sim 10$) leads to a transition with increasing frequency to much more strongly frequency-dependent dissipation ($\mathscr{L} \sim 1/\omega$) beyond $\omega \sim N^3/t_d$ resulting in a kink in the loss spectrum and the occurrence of a pronounced dissipation minimum on the low-frequency side of the viscous sliding peak described in (b) above. Physically, such a length scale can be imposed on grain corners if (e.g.) a second phase occurs there or, perhaps, if the sample contains pores. Because the location of the resulting kink is independent of the value of η', it cannot be used to infer a value for that parameter. Our analysis suggests that observed features that are currently interpreted as peaks superposed on an ill-defined 'background' might, in some cases, be simply corners in the spectrum.

(e) Lastly, at low frequencies ($\omega < 1/t_d$), $\mathscr{L} \sim 1/\omega$ as appropriate for steady-state (Coble) creep.

Though it has been suggested in the literature that to explain experiments, complications such as threshold stresses for diffusion may need to be incorporated into the Raj–Ashby model, we have chosen rather to analyse that model rigorously in its simplest non-trivial form. Our analysis shows that stress singularities at corners have a major effect on the high-frequency loss spectrum, and that effect needs to be explored in more realistic geometries. With the insight and quantitative results gained from the present small-slope analysis, in subsequent papers we will be able address that issue using numerical and asymptotic analysis.

We thank the reviewers for comments which have helped us to improve the presentation.

Appendix A. Interfacial conditions expressed in Cartesian form

The unit tangent and normal vectors $\boldsymbol{e_s}$, $\boldsymbol{e_n}$ are given in terms of $f'(x)$ by the expressions

$$\boldsymbol{e_s} = \boldsymbol{e_x}\frac{\mathrm{d}x}{\mathrm{d}s} + \varepsilon \boldsymbol{e_y}\frac{\mathrm{d}f}{\mathrm{d}s}, \tag{A.1a}$$

$$\boldsymbol{e_n} = \boldsymbol{e_y}\frac{\mathrm{d}x}{\mathrm{d}s} - \varepsilon \boldsymbol{e_x}\frac{\mathrm{d}f}{\mathrm{d}s}, \tag{A.1b}$$

$$\frac{\mathrm{d}x}{\mathrm{d}s} = 1/(1+\varepsilon^2 f'^2)^{1/2}. \tag{A.1c}$$

Using (A1), we may show that the interfacial conditions (6e)–(6h) are equivalent to the following:

$$\{1-\varepsilon^2 f'^2\}[\sigma_{xy}(x,\varepsilon f,\varepsilon)] + \varepsilon f'[\sigma_{yy}(x,\varepsilon f,\varepsilon) - \sigma_{xx}(x,\varepsilon f,\varepsilon)] = 0, \tag{A.2a}$$

$$\sigma_{nn}(x,\varepsilon f,\varepsilon) = \{\sigma_{yy}(x,\varepsilon f,\varepsilon) - 2\varepsilon f'\sigma_{xy}(x,\varepsilon f,\varepsilon) + \varepsilon^2 f'^2\sigma_{xx}(x,\varepsilon f,\varepsilon)\}/(1+\varepsilon^2 f'^2), \tag{A.2b}$$

$$\mathscr{M}\{[\dot{u}(x,\varepsilon f,\varepsilon)] + \varepsilon f'[\dot{v}(x,\varepsilon f,\varepsilon)]\}(1+\varepsilon^2 f'^2)^{1/2} = (1-\varepsilon^2 f'^2)\sigma_{xy}(x,\varepsilon f,\varepsilon) + \varepsilon f'\{\sigma_{yy}(x,\varepsilon f,\varepsilon) - \sigma_{xx}(x,\varepsilon f,\varepsilon)\}, \tag{A.2c}$$

$$[\dot{v}(x,\varepsilon f,\varepsilon)] = \varepsilon[\dot{u}(x,\varepsilon f,\varepsilon)]f' - \frac{\mathrm{d}}{\mathrm{d}x}((1+\varepsilon^2 f'^2)^{-1/2}\frac{\mathrm{d}}{\mathrm{d}x}\sigma_{nn}(x,\varepsilon f,\varepsilon)). \tag{A.2d}$$

Here, $\mathrm{d}/\mathrm{d}x$ denotes the total derivative. Eq. (A.2a) expresses continuity of the shear stress; (A.2b) gives the normal stress; and (A.2c) and (A.2d) are, respectively, the slip, and the diffusion, boundary conditions.

Appendix B. Mechanical energy balance on the sample

The two control volumes used in this argument are shown in Fig. 1. As shown there, the upper control volume $\mathscr{V}^+$ consists of one wavelength of the upper grain, with the grain interface excluded. The lower boundary of $\mathscr{V}^+$ consists of the surface s^+ lying immediately above the grain interface. The notation for the lower control volume is similar.

The balance of mechanical energy for the upper grain is obtained by contracting the equation of motion in the form

$$\frac{\partial \sigma_{ij}}{\partial x_j} = 0$$

with the velocity $\dot{u}_i = \partial u_i/\partial t$, integrating over the volume $\mathscr{V}^+$ of the upper grain and applying the divergence theorem. The result is

$$\lambda \dot{U}\tau = \int_{s^+} \dot{u}_i \sigma_{ij} n_j \mathrm{d}s + \int_{\mathscr{V}^+} \dot{e}_{ij}\sigma_{ij}\mathrm{d}\mathscr{V}. \tag{B.1}$$

Here, s denotes distance along the interface, and n_i is the unit normal pointing into the upper grain (as depicted in Fig. 1). Both integrands are evaluated within the upper grain. Eq. (B.1) relates the external power supplied at the upper sample boundary to the sum of two terms: namely, the rate of working by the upper grain on the lower grain, and the rate of increase of strain energy stored within the upper grain.

Forming a similar expression for the lower grain, we obtain

$$\lambda\dot{U}\tau = -\int_{s^-} \dot{u}_i\sigma_{ij}n_j\mathrm{d}s + \int_{\mathscr{V}^-} \dot{e}_{ij}\sigma_{ij}\mathrm{d}\mathscr{V}. \tag{B.2}$$

We let $\mathscr{V}$ be the union of the two time-independent volumes $\mathscr{V}^+$, V^- (with the interfacial region excluded). Adding (B.1) to (B.2) and recalling that $[\sigma_{ij}]n_j = 0$, we obtain the identity

$$2\lambda\dot{U}\tau = \int_s (\sigma_{nn}[\dot{u}_n] + \sigma_{ns}[\dot{u}_s])\mathrm{d}s + \dot{W}, \tag{B.3}$$

where the strain energy function W is defined by (52c). Eq. (52) follows by using Eqs. (1) and (2) to eliminate $[\dot{u}_s]$ and $[\dot{u}_n]$, then integrating by parts.

References

Barnhoorn, A., Jackson, I., Fitz Gerald, J.D., Aizawa, Y., 2007. Suppression of elastically accommodated grain-boundary sliding in high-purity MgO. J. Eur. Ceram. Soc. 27, 4697–4703.

Bland, D.R., 1960. Theory of Linear Viscoelasticity. Pergamon, New York.

Cooper, R.F., 2002. Seismic wave attenuation: energy dissipation in viscoelastic crystalline solids. In: Karato, S.-I., Wenk, H.-R. (Eds.), Plastic Deformation of Minerals and Rocks. Mineralogical Society of America, Washington, DC.

Davies, B., 1985. Integral Transforms and their Applications, second ed. Springer, Berlin.

Faul, U.H., Fitz Gerald, J.D., Jackson, I., 2004. Shear wave attenuation and dispersion in melt bearing olivine polycrystals. 2. Microstructural interpretation and seismological implications. J. Geophys. Res. 109, B06202.

Findley, W.N., Lai, J.S., Onaran, K., 1989. Creep and Relaxation of Nonlinear Viscoelastic Materials. Dover Publications, New York.

Ford, J.M., Ford, N.J., Wheeler, J., 2004. Simulation of grain-boundary diffusion creep: analysis of some new numerical techniques. Proc. R. Soc. Lond. A 460, 2395–2413.

Gribb, T.T., Cooper, R.F., 1998. Low frequency shear attenuation in polycrystalline olivine: grain boundary diffusion and the physical significance of the Andrade model for viscoelastic rheology. J. Geophys. Res. B 103, 27267–27279.

Hazzledine, P.M., Schneibel, J.H., 1993. Theory of Coble creep for irregular grain structures. Acta Metall. Mater. 41, 1253–1262.

Jackson, I., Fitz Gerald, J.D., Faul, U.H., Tan, B.H., 2002. Grain size sensitive seismic wave attenuation in polycrystalline olivine. J. Geophys. Res. 107 (B12), 2360.

Jackson, I., Faul, U.H., Fitz Gerald, J.D., Morris, S.J.S., 2006. Contrasting viscoelastic behaviour of melt-free and melt-bearing olivine: implications for the nature of grain-boundary sliding. Mater. Sci. Eng. A 442, 170–174.

Kim, B.-N., Hiraga, K., Morita, K., 2005. Viscous grain-boundary sliding and grain rotation accommodated by grain-boundary diffusion. Acta Mater. 53, 1791–1798.

Lakki, A., Schaller, R., Carry, C., Benoit, W., 1999. High-temperature anelastic and viscoplastic deformation of fine-grained magnesia- and magnesia/yttria-doped alumina. J. Am. Ceram. Soc. 82, 2181–2187.

Lee, L.-C., Jackson, I., Morris, S., Zohdi, T., 2007. A finite element study of elastically accommodated grain boundary sliding. Eos Trans. AGU 88 (52) Fall Meet. Suppl. Abstract MR13C-02.

Lifshitz, I.M., 1963. On the theory of diffusion-viscous flow of polycrystalline solids. Sov. Phys. JETP 17, 909–920.

Morris, S.J.S., Jackson, I., 2008. Implications of the similarity principle relating creep and attenuation in fine-grained solids. Mater. Sci. Eng. A, to appear (International Congress on Internal Friction and Mechanical Spectroscopy (ICIFMS), Perugia 2008).

Mosher, D.R., Raj, R., 1974. Use of the internal friction technique to measure rates of grain boundary sliding. Acta Metall. 22, 1469–1474.

Nowick, A.S., Berry, B.S., 1972. Anelastic Relaxation in Crystalline Solids. Academic, New York.

O'Connell, R.J., Budiansky, B., 1978. Measures of dissipation in viscoelastic media. Geophys. Res. Lett. 5, 5–8.

Pezzotti, G., Ota, K., Kleebe, H.-J., 1996. Grain boundary relaxation in high-purity silicon nitride. J. Am. Ceram. Soc. 79, 2237–2246.

Picu, C.R., Gupta, V., 1996. Stress singularities at triple junctions with freely sliding grains. Int. J. Solids Struct. 33, 1535–1541.

Raj, R., Ashby, M.F., 1971. On grain boundary sliding and diffusional creep. Metall. Trans. 2, 1113–1127.

Raj, R., 1975. Transient behaviour of diffusion-induced creep and creep rupture. Metall. Trans. A 6, 1499–1509.